Direct-write microfabrication of single-chamber micro solid oxide fuel cells

2008 J. Micromech. Microeng. 18 015005

(http://iopscience.iop.org/0960-1317/18/1/015005)

J. Micromech. Microeng. **18** (2008) 015005 (8pp) doi:10.1088/0960-1317/18/1/015005

Direct-write microfabrication of single-chamber micro solid oxide fuel cells

Melanie Kuhn[1], Teko Napporn[2], Michel Meunier[2], Srikar Vengallatore[3] and Daniel Therriault[1]

[1] Department of Mechanical Engineering, École Polytechnique de Montréal, Montreal, H3T 1J4, Canada
[2] Department of Engineering Physics, École Polytechnique de Montréal, Montreal, H3T 1J4, Canada
[3] Department of Mechanical Engineering, McGill University, Montreal, H3A 2K6, Canada

E-mail: daniel.therriault@polymtl.ca

Received 31 May 2007, in final form 11 September 2007
Published 28 November 2007
Online at stacks.iop.org/JMM/18/015005

Abstract

Single-chamber micro solid oxide fuel cells (SC-μSOFCs) are promising systems for portable power generation. Here we report the direct-write microfabrication and electrochemical testing of SC-μSOFCs in the single-face configuration which consists of closely spaced interdigitated electrodes on an electrolyte substrate. In direct-write microfabrication, powdered electrode materials are first synthesized into inks which are subsequently extruded through a micronozzle onto an electrolyte plate mounted on a robot-controlled platform. The microfabricated structures are then sintered to remove the organic components of the inks and to obtain porous electrodes. Processing–structure relationships were obtained using systematic experimentation for the direct-write microfabrication of nickel oxide–yttria stabilized zirconia (NiO–YSZ) anodes and lanthanum strontium manganite (LSM) cathodes on an YSZ electrolyte. Single-chamber μSOFCs were fabricated with interdigitated electrodes of a few hundred microns in size. When tested in a fuel–air mixture (methane-to-oxygen ratio $R_{\mathrm{mix}} = 2$) at a furnace temperature of 700 °C, the cells exhibited an open circuit voltage of 800 mV and a peak power density of $\sim$1 mW cm^{-2}. Implications for the use of these devices for portable power generation are discussed.

(Some figures in this article are in colour only in the electronic version)

1. Introduction

Miniaturized fuel cells are attractive candidates for portable power generation to enable the operation of electronic devices and microelectromechanical systems (MEMS). Compared with conventional electrochemical batteries, micro fuel cells are capable of higher energy densities and lower recharging times. Research in this relatively new field currently focuses on two major categories of fuel cells, namely, polymer-based proton-exchange membrane (PEM) fuel cells operating at low temperatures of 20–100 °C [1], and ceramic-based solid oxide fuel cells (SOFCs) requiring significantly higher temperatures of 500–1000 °C for efficient operation [2]. PEM fuel cells are restricted to operate only on hydrogen or methanol fuels, whereas SOFCs can operate on a wide range of hydrocarbon fuels with greater energy densities and without the need of expensive catalysts.

The first type of micro solid oxide fuel cells (μSOFCs) explored was a traditional dual-chamber design in which an electrolyte layer is sandwiched between porous anode and cathode layers [3]. The term dual chamber refers to the operating mode wherein the two reactant gases—fuel (hydrogen or hydrocarbons) and oxidant (oxygen or air)—are fed to the anode and to the cathode, respectively, without any intermixing. Significant progress has been made in thin-film microfabrication of fuel cell components and in structural design of dual-chamber micro fuel cells [3, 4]. However, this experience has also highlighted several significant difficulties in the miniaturization of the dual-chamber design including (i) developing high-temperature microfluidic sealing technologies to keep the two gas streams separated [5];

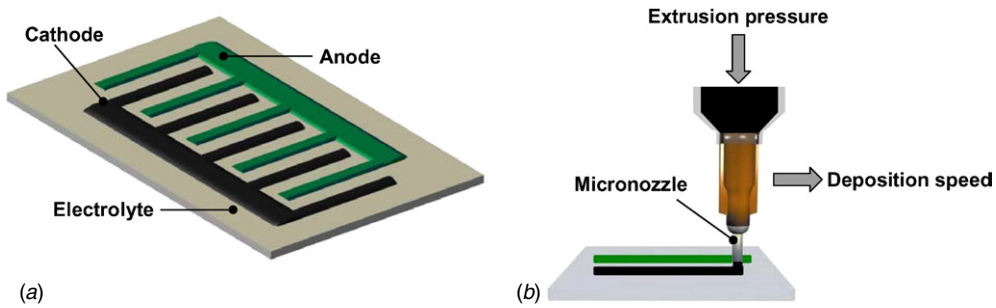

Figure 1. (*a*) Schematic illustration of a single-chamber solid oxide fuel cell in single-face configuration with interdigitated electrodes. (*b*) Schematic illustration of the robot-controlled direct-write microfabrication of electrode lines on an electrolyte plate. The quality of the deposited structures strongly depends on the two main process parameters, extrusion pressure and deposition speed.

(ii) controlling intrinsic residual stresses in vapour-phase-deposited thin films of electrodes and electrolytes; and (iii) ensuring thermomechanical stability and minimizing thermal losses in the design of the thin three-layer sandwich structure [3, 4].

The difficulties encountered with miniaturizing dual-chamber designs motivated us to explore an alternate concept of single-chamber micro SOFCs (SC-μSOFCs). In this operating mode, the fuel and air streams are pre-mixed, and the mixture is allowed to flow over both electrodes. The operation of the device relies upon selective reactions at the anode and cathode in terms of oxidation and reduction processes. The single-chamber concept dates back to the 1950s [6] and 1960s [7], but it was only recently that this operating mode has been investigated for SOFCs [8, 9]. Several configurations of single-chamber SOFCs have been proposed including the traditional three-layer sandwich structure (with the electrolyte contained between the two electrodes) [8–10], a flow-through structure with a fully porous electrolyte and electrodes [11], and planar single-face configurations in which both electrodes are patterned on the same side of the electrolyte [12–14].

Figure 1(*a*) shows a schematic illustration of a planar SC-μSOFC in the single-face configuration, in which interdigitated patterns of the anode and cathode are fabricated on the same surface of a thick electrolyte plate. This configuration is particularly appealing for miniaturization because the use of pre-mixed air and fuel streams eliminates the need for gas-tight microfluidic sealing. In addition, a thick electrolyte can be used without any penalties on electrochemical performance, while ensuring mechanical strength and stability during operation at high temperatures. Finally, the planar configuration is suited for parallel or serial connection of multiple individual micro fuel cells on the same electrolyte substrate, as well as for integration with microsensors and microactuators used in MEMS technology.

Experimental work [12–14] on SC-μSOFCs in the single-face configuration and modelling [15] suggest that minimized ohmic resistance for surface ionic conduction and optimal electrochemical performance are achieved by reducing the inter-electrode spacing between the adjacent anode and cathode structures to the order of a few tens of micrometers. Additionally, porous electrodes are required to maximize the number of gas/electrode/electrolyte triple-phase boundaries for the electrochemical reactions. However, these requirements, especially the synthesis of thick porous electrodes using multicomponent ceramics, are largely incompatible with traditional thin-film processing and photolithography-based microfabrication. Hence, alternate methods of microfabrication, such as screen printing [16], soft lithography [17] and direct-write microfabrication [14, 18], are being explored for the synthesis of high-performance SC-μSOFCs.

In this paper, we present a detailed report of direct-write microfabrication, structural characterization and electrochemical testing of SC-μSOFCs. The essential principles and challenges of direct-write microfabrication, and the key process parameters associated with this method are discussed in section 2. Section 3 presents an experimentally determined process map for direct-write microfabrication of ceramic structures. Section 4 describes the synthesis and characterization of interdigitated micro-electrodes on an electrolyte substrate using an optimal set of process parameters. Finally, the electrochemical testing of fabricated SC-μSOFCs in methane–air mixtures is presented in section 5.

2. Principles of direct-write microfabrication

The direct-write microfabrication technique used here refers to the pressure-driven extrusion of an ink (or suspension) through a micronozzle and its robot-controlled deposition on a suitable substrate, as schematically illustrated in figure 1(*b*). This technique enables rapid, repeatable and potentially low-cost manufacturing of complex shapes and patterns [19, 20]. The primary steps in the direct-write microfabrication of ceramic or metallic electrodes for single-chamber solid oxide fuel cells in single-face configuration are as follows. First, the electrode materials are obtained in the form of powders and processed to synthesize suspensions (or inks) of the desired viscosity. Next, the inks are deposited onto an electrolyte plate by means of pressure-driven extrusion through a micronozzle at room temperature. This plate is mounted on a robot-controlled mobile platform, which permits the deposition of electrodes of different two-dimensional shapes and sizes. After deposition, the electrode structure is sintered to remove the organic components of the inks and to obtain porous electrodes.

The direct writing of SC-SOFCs involves numerous parameters such as the particle size and size distribution of

the electrode powders, rheological properties of the inks, the extrusion parameters (micronozzle diameter, extrusion pressure), the deposition parameters (deposition speed) and the sintering time and temperature. An optimal selection of these material and process parameters is essential in order to achieve continuous and uniform deposits of specified dimensions and with a homogeneous microstructure. Consider first the preparation of the ceramic inks. The rheological properties (specifically, viscosity and storage modulus) govern the flow of the ink through the nozzle during deposition and dictate the extent to which the extruded shape is retained after deposition [21]. In turn, the rheological properties of the inks are dominated by the particle loading, ϕ, (i.e., weight fraction of electrode powders). Previous studies [22] suggest that the particle loading must be chosen so as to (i) permit uniform flow of inks through the nozzle during extrusion, (ii) retain shape after deposition, (iii) minimize shrinkage and damage during drying and sintering and to (iv) obtain a homogeneous porous microstructure with a percolating interconnected particle network after high-temperature sintering. Consideration of these factors suggests an optimal range of $0.5 < \phi < 0.6$ [22]. Our preliminary experiments indicate that, for higher solid loadings, the suspension easily clogs the micronozzle during extrusion and exhibits poor flow characteristics. Conversely, for lower values of ϕ, the ink is easily extruded but the deposit will not retain its shape and size after extrusion. Also, a non-percolating microstructure with poorly bonded particles can result after sintering.

Once the ink is prepared, the direct-write process parameters, namely, extrusion pressure and deposition speed, must be considered. Optimal deposition is achieved when the deposited structures are uniform, continuous, and exhibit an average width, w_{av}, that is comparable to the inner diameter of the extrusion micronozzle, w_{nozzle}. For a given deposition speed, the deposited structures are expected to be discontinuous for low extrusion pressures, but oversized ($w_{av} > w_{nozzle}$) for high pressures. Similar arguments hold for deposition under fixed extrusion pressure and varying deposition speeds. Hence, it is expected that there exist optimal ranges of direct-write process parameters over which uniform deposits of the desired size can be obtained. However, reliable quantitative estimates for these ranges have not yet been established. This motivated us to undertake a series of systematic experiments to identify the ranges of viscosities, extrusion pressures and deposition speeds that lead to optimal deposited structures.

3. Experimental details and process maps

3.1. Preparation of electrode suspensions

The electrode materials were obtained from NexTech Materials in the form of NiO–YSZ (8 mol% yttria) powder (a median particle size of 0.9 μm, specific surface area (BET-surface) of 2.071 $m^2\ g^{-1}$, weight ratio of NiO:YSZ of 60:40) and $(La_{0.8}Sr_{0.2})_{0.98}MnO_3$ powder (a median particle size of 0.6 μm and a specific surface area (BET-surface) of 4.2438 $m^2\ g^{-1}$). In addition, an anode powder with a weight ratio of NiO:YSZ = 55:45 was also prepared. Anode and cathode suspensions with different particle loadings between 36 wt% and 60 wt% were prepared by ball milling for 1 h with YSZ balls (5–10 mm in diameter) in a Spex Mixer/Mill (Spex 8000 M), using α-Terpineol as solvent, Tritton as dispersant and polyvinyl butyral (PVB) as dispersant.

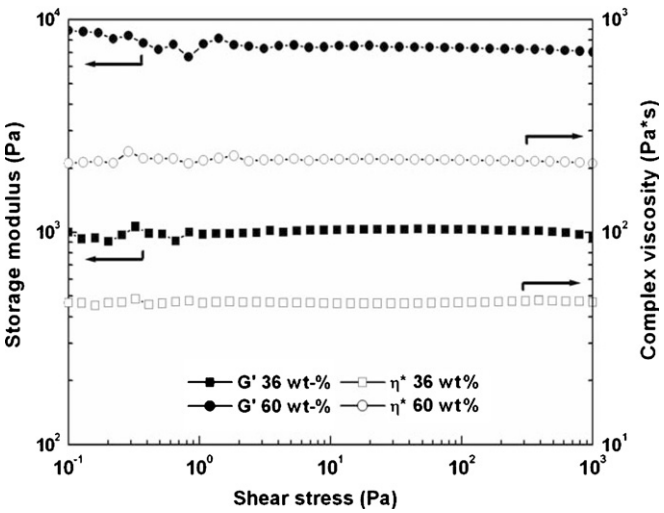

Figure 2. Rheological properties (storage modulus G' and complex viscosity η^*) of anode suspensions with two different particle loadings as a function of shear stress at a frequency of 10 Hz.

3.2. Rheological characterization

The viscosity and rheological behaviour of ink suspensions are critical for their successful pressure-driven extrusion through a micronozzle [21]. The rheological characterization of anode suspensions with different particle loadings was performed at room temperature on a controlled stress oscillatory rheometer (Bohlin CVO 120) using a parallel plate geometry (the diameter of the upper plate was 25 mm). An amount of about 1 mL of the different suspensions was used for the measurements. The complex shear modulus (composed of the storage and the loss modulus, G' and G'') and the complex viscosity, η^*, were measured as a function of stress in an oscillatory shear stress amplitude sweep at a frequency of 10 Hz. A constant viscosity and shear modulus were observed for all suspensions over the applied shear stress range. Figure 2 presents a comparative graph of the storage modulus and complex viscosity as functions of the shear stress amplitude for two different suspensions with particle loadings of $\phi = 0.36$ and $\phi = 0.6$. A significant increase of both storage modulus and viscosity with increasing particle loading is evident. Following the guidelines developed by Cesarano *et al* [22], we focused on the inks with high particle loadings for the direct-write microfabrication of electrode structures.

3.3. Direct-write process map

A photograph of the direct-writing system is shown in figure 3. The electrode suspensions were filled in syringes (volume = 3 cm^3, barrel diameter = 9.6 mm, EFD Inc.) and extruded

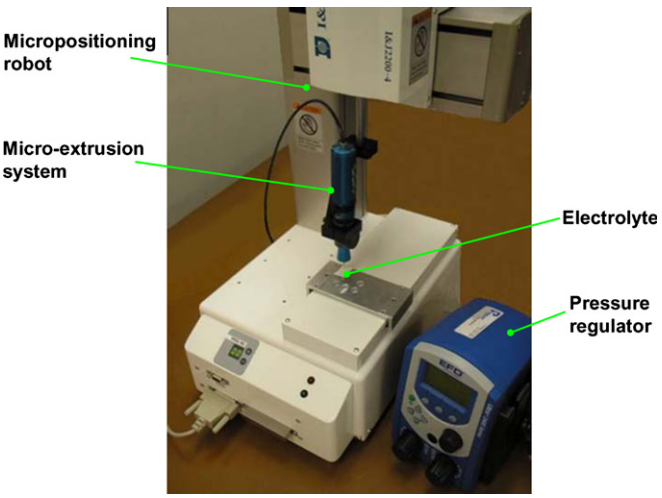

Figure 3. Picture of the direct-write microfabrication setup. The sample is mounted on a translation stage, and the micro-extrusion system on a robotic arm permits writing of arbitrary shapes.

through high precision stainless steel micronozzles (EFD Inc.) using a pressure regulator (Ultra^{TM} 2400 series, EFD Inc.) combined with an air-powered micro-extrusion system (HP7x, EFD Inc.), which enabled a maximum pressure of 49 bar. Micronozzles with different inner diameters (100, 150 and 330 μm) were used. The combination of the micro-extrusion system with a robotic deposition apparatus (I & J 2200-4, I & J Fisnar Inc.) enabled the deposition of the extruded suspensions onto an yttria-stabilized zirconia (YSZ) plate (0.2 mm thick, Marketech International). The pattern for direct writing was programmed using the software JR points for dispensing (Version 4.85E, Janome Sewing Machine Co., Ltd). An optical microscope was used for *in situ* observation of the extrusion and deposition process.

Figure 4 shows a representative process map that was obtained from the analysis of several straight electrode lines deposited under different combinations of extrusion pressure and deposition speed. All depositions were performed using a 60 wt% anode suspension extruded through a micronozzle with an inner diameter of 150 μm. Optical micrographs of the deposited anode lines were obtained with an Olympus SZX12 stereomicroscope and an Evolution^{TM} VF colour camera with 1.4 million pixel resolutions. Straight lines of the anode suspension were deposited at five different speeds (0.1, 0.2, 0.3, 0.4 and 0.5 mm s^{-1}) and at pressures ranging from 5.6 to 11.2 bar. At low extrusion pressures and at elevated deposition speeds, the deposited lines are discontinuous. For high pressures and low speeds, the width of the deposited lines is significantly larger than the micronozzle diameter, resulting in broadened lines. Multiple optimal combinations of extrusion pressures and speeds can also be identified that lead to the deposition of narrow, continuous lines, and an optimal zone is shown in the process map.

Several practical considerations impact the selection of a few optimal combinations from this set. The structures of interest are only a few millimetres in length and, therefore, only a few minutes are required for deposition even at low deposition speeds in the range of 0.1 mm s^{-1}. However, the pressure corresponding to this speed is low and subject to fluctuations during deposition using our dispensing system. In contrast, at significantly higher velocities (>0.6 mm s^{-1}), there is a reduced control in the deposition of short structures. Hence, speeds in the range of 0.2–0.5 mm s^{-1}, and the

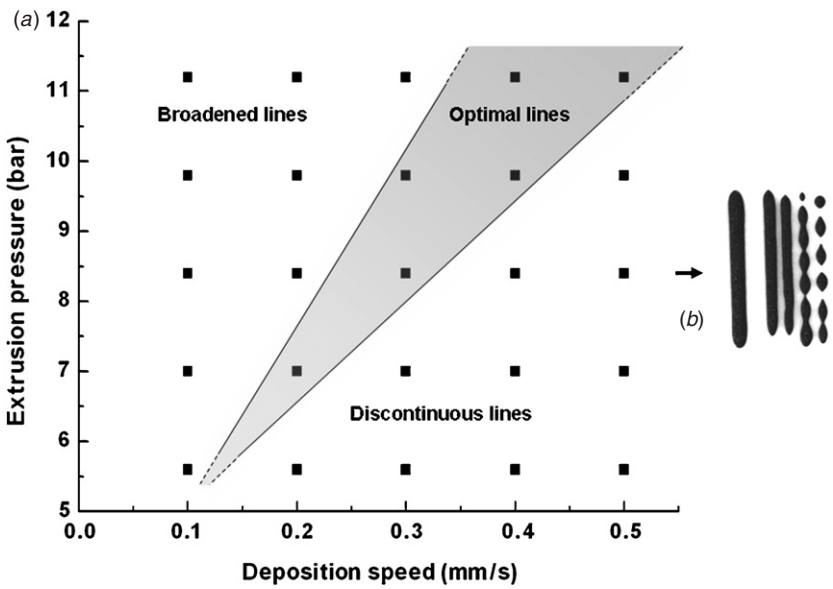

Figure 4. (*a*) Representative process map for direct-write microfabrication of anode lines with axes corresponding to extrusion pressure and deposition speed. The 60 wt% anode suspension was extruded through a micronozzle with an inner nozzle diameter of 150 μm. Optimal deposits with uniform, continuous lines were obtained for pressure–speed combinations within the grey area. (*b*) Optical micrograph corresponding to an extrusion pressure of 8.4 bar. From left to right, the single lines correspond to the deposition speed of 0.1, 0.2, 0.3, 0.4 and 0.5 mm s^{-1}, respectively.

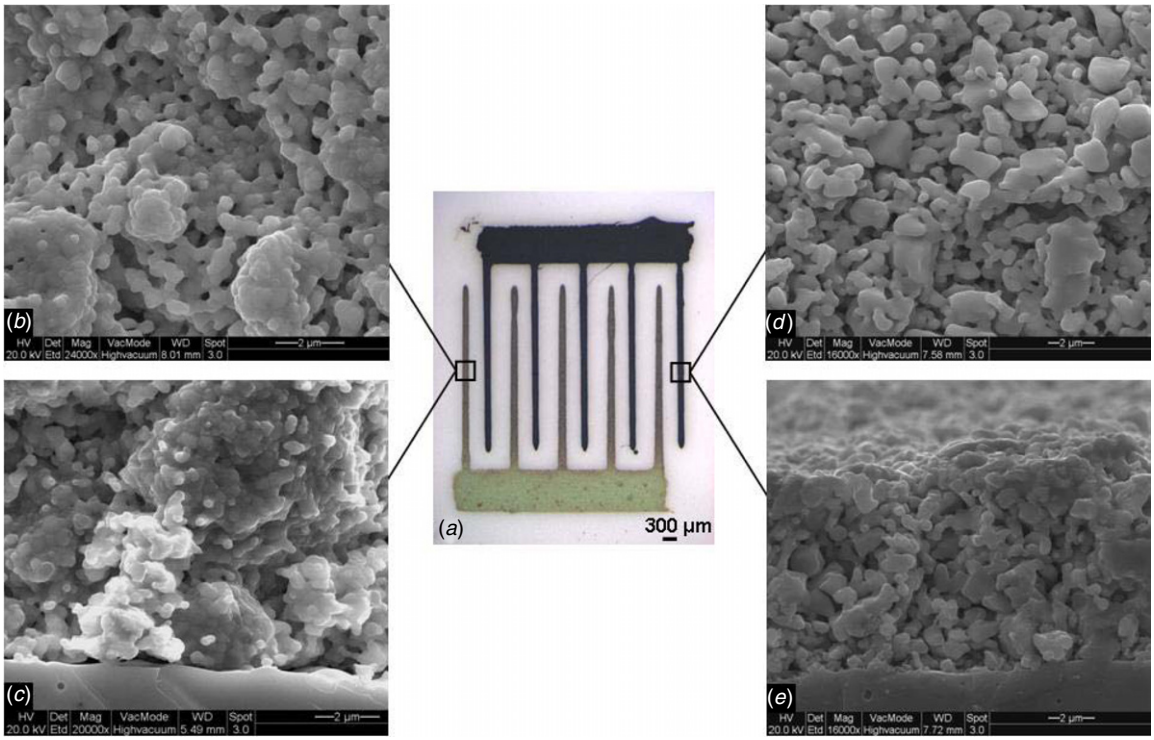

Figure 5. (*a*) Optical micrograph of SC-μSOFC with interdigitated electrodes fabricated by the direct-write technique. SEM images of the anode microstructure in top (*b*) and cross-sectional view (*c*). SEM microstructure characterization of the cathode in top (*d*) and cross-sectional view (*e*).

Table 1. Average electrode line width w_{av} and standard deviation σ for anode and cathode lines of the SC-μSOFC from figure 5(*a*). The lines are numbered from the left to the right. All values are given in μm. One pixel in the image corresponds to 5.6 μm. A micro-nozzle with an inner nozzle diameter of 100 μm was used for the direct-write microfabrication of the electrode structures.

	Line 1		Line 2		Line 3		Line 4		Line 5	
	w_{av}	σ	w_{av}	σ	w_{av}	σ	w_{av}	σ	w_{av}	σ
Anode	124	11	138	16	146	12	142	14	133	21
Cathode	130	9	125	7	133	7	122	9	117	7

corresponding pressures in the range of 7–11 bar, were used for optimal deposition.

Importantly, the optimal process parameters identified in figure 4 pertain only to the microfabrication of uniform, continuous, narrow electrodes by direct-write microfabrication. The next step is to enquire whether such structures lead to optimal electrochemical performance, efficiency and reliability. As the first step toward the goal of formulating robust process–structure–performance–reliability correlations, the following section describes the microfabrication and testing of SC-μSOFCs.

4. Fabrication and structural characterization of SC-μSOFCs

After optimizing the direct-write process parameters to achieve uniform and continuous electrode structures, SC-μSOFCs in single-face configuration were fabricated. A deposition speed of 0.3 mm s^{-1} and an extrusion pressure of 8.4 bar, as identified from the optimal zone in figure 4, were used for the fabrication of both anode and cathode structures. The anode structures were deposited first on the YSZ plate using a 60 wt% anode suspension and then were sintered at 1250 °C for 3 h under ambient atmosphere in a chamber furnace. Subsequently, the cathode structures were deposited by extruding a suspension with a particle loading of 57 wt%, and the fuel cell device was sintered at 1100 °C for 3 h.

Several micro solid oxide fuel cells were manufactured with inter-electrode spacings ranging from 37 μm to 846 μm, and average electrode widths ranging from 125 μm to 316 μm. These values of inter-electrode spacing and electrode width were obtained from optical imaging analysis (Image-Pro Plus 6.2, MediaCybernetics) and were confirmed by profilometry of the electrode structures. Figure 5(*a*) shows a representative example of a SC-μSOFC with interdigitated pairs of five anode and five cathode lines. The average inter-electrode spacing of this cell is 300 μm. The width of each electrode line was measured at 20 different locations, and the mean value and standard deviation are reported in table 1. These values provide an indication of the stability of the direct-write process during microfabrication of the anode and cathode. The average anode and cathode width are 137 μm and

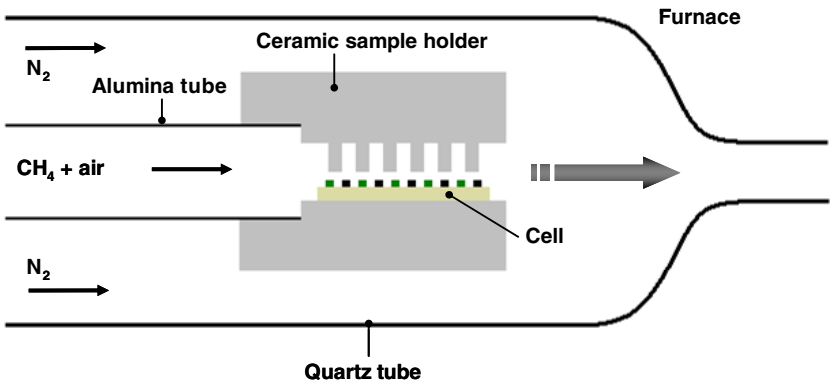

Figure 6. Schematic of the electrochemical testing setup. The cell is placed in a ceramic holder inside a quartz tube. The methane–air mixture is supplied to the cell through an inner alumina tube. Additional nitrogen is used as carrier gas and to avoid counter-diffusion.

125 μm, respectively. A micro-nozzle with an inner nozzle diameter of 100 μm was used for the direct-write fabrication of this cell.

The microstructure and thickness of the sintered electrodes were characterized using a Quanta FEG 200 (FEI Instruments) scanning electron microscope (SEM) with the software xT Microscope control and xT Docu (FEI Instruments). Figures 5(*b*)–(*e*) show the SEM micrographs for both electrodes in plan and cross-sectional view, revealing a porous and homogeneous microstructure for anode and cathode. The thickness of the electrodes varies from 10 to 30 μm in different cells. At lower magnification, the cross-sectional images reveal that the electrode sidewalls are not vertical, but instead exhibit rounded edges. This lens-like shape is due to the spreading of the inks on the substrate after deposition. Optimizing the direct-write method and tailoring the rheological properties of the inks, to reduce the wetting of the substrate by the inks and to achieve thicker and uniform electrodes with reduced inter-electrode spacings, remains an open question that will be addressed in our future efforts.

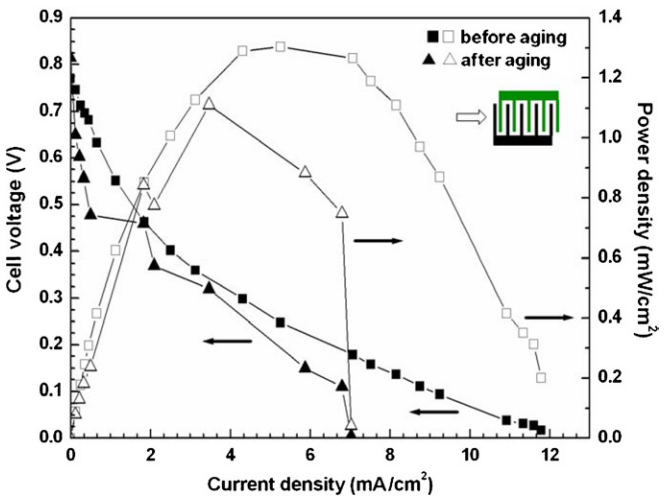

Figure 7. Polarization curve of SC-μSOFC with interdigitated electrodes (average inter-electrode spacing of 517 μm) at 700 °C, a total gas flow of 150 sccm and a methane-to-oxygen ratio $R_{\mathrm{mix}} = 2$. The results before and after an ageing period of 24 h are shown.

5. Electrochemical testing

Electrochemical characterization of the fabricated SC-μSOFCs was performed using a high-temperature test station that is shown schematically in figure 6 and is described in detail in [23]. The cell was located in a ceramic sample holder inside a quartz tube, and a methane–air mixture was allowed to flow over the cell at a total gas flow of 150 sccm. The characteristic value associated with the gas mixture is the methane-to-oxygen ratio R_{mix}. The electrode lines were orientated perpendicular to the gas flow. Nitrogen was used as a carrier gas to prevent any counter-flow. Gold wire and grid (Alfa Aesar) fixed with gold paste (paste C5450 from Heraeus, Inc.) served as a current collector. The furnace temperature was set to 700 °C, and the cell potential was recorded as a function of the electrical current drawn from the micro fuel cell.

Figure 7 shows the results of a test using a micro fuel cell in which the average inter-electrode distance was 517 μm, and the surface area per electrode was 0.22 cm^2. The anode had an average width and thickness of 320 μm and 27 μm, respectively, and the corresponding values for the cathode were 130 μm and 10 μm, respectively. The vertical axes of the graph correspond to the cell voltage and power density, and the horizontal axis is the current density. Both power and current were normalized by the electrode surface area of 0.22 cm^2. At $R_{\mathrm{mix}} = 2$, an open circuit voltage (OCV) of ~800 mV was rapidly obtained. For comparison, the theoretical maximum OCV is 1.23 V. A maximum power density of 1.3 mW cm^{-2} and a maximum current density of 12 mA cm^{-2} were also measured (figure 7).

The cell was tested in open circuit for 24 h in the methane–air mixture ($R_{\mathrm{mix}} = 2$) at 700 °C to characterize its long-term stability. The open circuit voltage was monitored as a function of time. It shows oscillations between 400 mV and 800 mV (figure 8). Jacques-Bédard *et al* [24] have previously suggested oxidation–reduction cycles of the anodic nickel as a probable cause of these oscillations. After this ageing test, the cell was polarized again. Although there was no significant change in the OCV, a degradation of the performance was noted (figure 7). The peak power density dropped by 15% to 1.1 mW cm^{-2}, and the maximum current density decreased by 41% to about 7 mA cm^{-2}. As observed by Jacques-Bédard

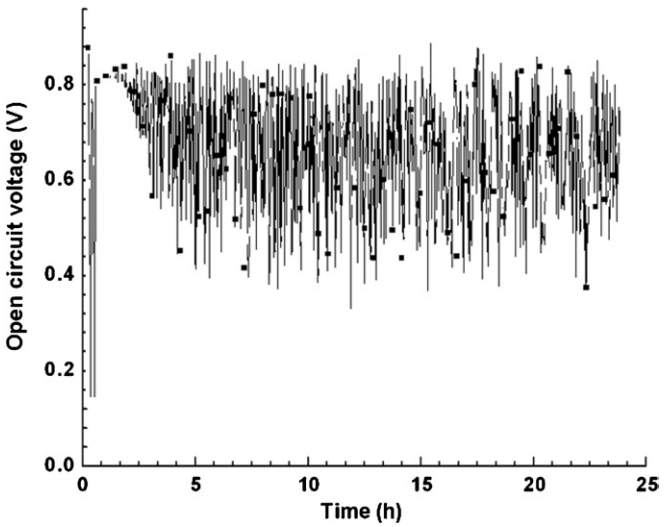

Figure 8. Open circuit voltage (OCV) as a function of time for ageing of a direct-written SC-μSOFC at 700 °C, $R_{mix} = 2$ and a total gas flow of 150 sccm. No current load was applied.

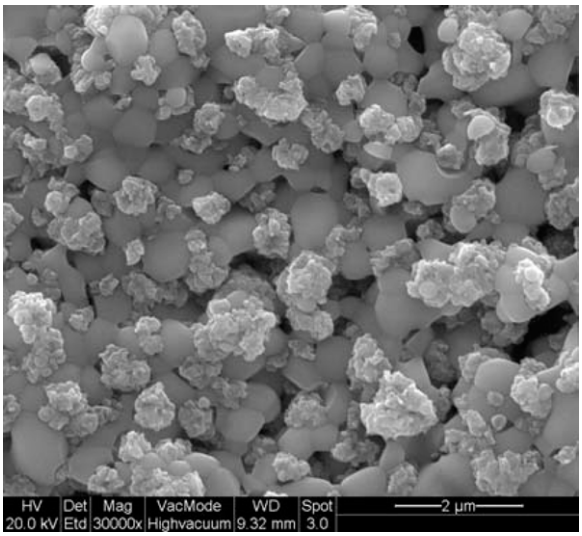

Figure 9. Scanning electron micrograph of the anode after electrochemical testing. The bright flake-like regions consist of metallic nickel.

et al [24], this performance decrease is due to the partial loss of nickel at the anode by transformation into volatile $Ni(OH)_2$.

The characterization of the anode microstructure after electrochemical testing indicated that the nickel oxide had been reduced to metallic nickel in the reducing atmosphere of the testing furnace. The flake-like structures in the SEM image shown in figure 9 were identified as nickel using energy-dispersive x-ray analysis.

At this stage, it is instructive to compare our results with those reported in the literature for the performance of single-chamber SOFCs. As compiled in a recent review by Yano *et al* [25], values for the peak power density range from 1 mW cm^{-2} to 100 mW cm^{-2} at temperatures between 700 and 900 °C. Unfortunately, a direct one-to-one comparison of results is not possible because of subtle, but critical, differences in the materials used for electrodes and electrolytes, differences in electrode architectures and dimensions, use of different test conditions (especially, the ratio of fuel and air in the gas mixture, furnace temperature and the flow direction with respect to electrode geometry) and differences in the design of the setup used for electrochemical testing.

As an illustrative example of the importance of such differences, we compare the OCV between different sets of SC-μSOFCs in the single-face configuration manufactured using direct-write microfabrication. Recently, Ahn *et al* [14] tested such fuel cells with interdigitated electrodes in a methane–air mixture at 900 °C, and reported the OCV values of ∼800 mV and 540 mV for cells with one pair and four pairs of electrodes, respectively. In contrast, in our fuel cells, a relatively high OCV of 800 mV is obtained at 700 °C even in structures with five pairs of interdigitated electrodes. In addition, the OCV fluctuates periodically between 400 mV and 800 mV as a function of time in ageing tests. Importantly, the electrolyte (YSZ) and cathode (LSM) are nominally identical in all these fuel cells. However, the anodes used by Ahn *et al* [14] were a mixture of NiO, gadolinium-doped ceria and metallic Pd, whereas our fuel cells used a mixture of NiO and YSZ for the anode. Thus, taken together, these results highlight the importance of subtle material and geometric parameters in determining the performance of SC-μSOFCs.

6. Summary

A direct-write microfabrication method has been used for the manufacture of single-chamber micro solid oxide fuel cells with interdigitated electrodes. The method is simple in concept, but involves numerous process parameters. Process–structure correlations were obtained experimentally and catalogued in the form of process maps. Specifically, the effects of particle loading on viscosity, and the effects of extrusion pressure and deposition speed on the geometry and quality of the deposited structures were elucidated. Single-chamber μSOFCs were fabricated with NiO–YSZ anode and LSM cathode on an YSZ electrolyte. Scanning electron microscopy confirmed the formation of homogeneous, porous electrodes after sintering. The fabrication process is quick and stable. Electrochemical testing showed an OCV of ∼800 mV at 700 °C. An important conclusion is that a high OCV can be achieved even with multiple interdigitated electrodes.

This work provides a foundation for further exploration of single-chamber μSOFCs. Specifically, we intend to investigate the effects of testing conditions on electrochemical performance, and the synthesis and testing of cells with different electrode geometries and sizes. The long-term goal of these activities is to develop detailed processing–structure–performance–reliability correlations for single-chamber μSOFCS developed by direct-write deposition. Such correlations will help in evaluating the benefits of this technology for portable power generation and for integration with microsystems employed in harsh high-temperature environments.

Acknowledgments

The authors gratefully acknowledge funding for this project by the Fonds Québécois de la Recherche sur la Nature et les Technologies (FQRNT) and the Canadian Foundation for Innovation. Financial support for M Kuhn was provided by the government of Québec (Doctoral research scholarship by FQRNT).

References

[1] Nguyen N T and Chan S H 2006 Micromachined polymer electrolyte membrane and direct methanol fuel cells—a review *J. Micromech. Microeng.* **16** R1–12
[2] Minh N Q and Takahashi T 1995 *Science and Technology of Ceramic Fuel Cells* (Amsterdam: Elsevier)
[3] Srikar V T, Turner K T, Ie T Y A and Spearing S M 2004 Structural design considerations for micromachined solid-oxide fuel cells *J. Power Sources* **125** 62–9
[4] Tang Y, Stanley K, Wu J, Ghosh D and Zhang J 2005 Design consideration of micro thin film solid-oxide fuel cells *J. Micromech. Microeng.* **15** S185–92
[5] Shim D J, Sun H W, Vengallatore S T and Spearing S M 2006 Damage and failure in silicon-glass-metal microfluidic joints for high-pressure MEMS devices *J. Microelectromech. Syst.* **15** 246–58
[6] Grueneberg G 1965 *Fuel Cells: Modern Processes for the Electrochemical Production of Energy* (New York: Wiley-Interscience) pp 362–89
[7] Eyraud C, Lenoir J and Gery M 1961 Fuel cells using electrochemical properties of adsorbents *C. R. Acad. Sci.* **252** 1599–600
[8] Hibino T, Hashimoto A, Inoue T, Tokuno J, Yoshida S and Sano M 2000 A low-operating-temperature solid-oxide fuel cell in hydrocarbon–air mixtures *Science* **288** 2031–3
[9] Napporn T W, Jacques-Bedard X, Morin F and Meunier M 2004 Operating conditions of a single-chamber SOFC *J. Electrochem. Soc.* **151** A2088–94
[10] Shao Z, Haile S M, Ahn J, Ronney P D, Zhan Z and Barnett S A 2005 A thermally self-sustained micro solid-oxide fuel-cell stack with high power density *Nature* **435** 795–8
[11] Suzuki T, Jasinski P, Petrovsky V, Anderson H U and Dogan F 2005 Performance of a porous electrolyte in single-chamber SOFCs *J. Electrochem. Soc.* **152** A527–31
[12] Hibino T, Ushiki K and Kuwahara Y 1996 New concept for simplifying SOFC system *Solid State Ion.* **91** 69–74
[13] Jacques-Bedard X, Napporn T W, Roberge R and Meunier M 2007 Coplanar electrodes design for a single-chamber SOFC: assessment of the operating parameters *J. Electrochem. Soc.* **154** B305–9
[14] Ahn S J, Kim Y B, Moon J, Lee J H and Kim J 2006 Co-planar type single chamber solid oxide fuel cell with micro-patterned electrodes *J. Electroceram.* **17** 689–93
[15] Fleig J, Tuller H L and Maier J 2004 Electrodes and electrolytes in micro-SOFCs: a discussion of geometrical constraints *Solid State Ion.* **174** 261–70
[16] Yoon S P, Kim H J, Park B T, Nam S W, Han J, Lim T H and Hong S 2006 Mixed-fuels fuel cell running on methane–air mixture *J. Fuel Cell Sci. Technol.* **3** 83–6
[17] Ahn S J, Lee J H, Kim J and Moon J 2006 Single-chamber solid-oxide fuel cell with micropatterned interdigitated electrodes *Electrochem. Solid-State Lett.* **9** A228–31
[18] Kuhn M, Napporn T, Meunier M, Therriault D and Vengallatore S 2007 Direct-write microfabrication of single-chamber solid oxide fuel cells with interdigitated electrodes *Mater. Res. Soc. Symp. Proc.* **972** 211–6
[19] Lewis J A 2002 Direct-write assembly of ceramics from colloidal inks *Curr. Opin. Solid State Mater. Sci.* **6** 245–50
[20] Therriault D, White S R and Lewis J A 2003 Chaotic mixing in three-dimensional microvascular networks fabricated by direct-write assembly *Nat. Mater.* **2** 265–71
[21] Karis T E 1996 An overview of rheology in the computer industry *J. Appl. Polym. Sci.* **59** 1405–16
[22] Cesarano J, Segalman R and Calvert P 1998 Robocasting provides moldless fabrication from slurry deposition *Ceram. Ind.* **148** 94–102
[23] Napporn T, Morin F and Meunier M 2004 Evaluation of the actual working temperature of a single-chamber SOFC *Electrochem. Solid-State Lett.* **7** A60–2
[24] Jacques-Bedard X, Napporn T W, Roberge R and Meunier M 2006 Performance and ageing of an anode-supported SOFC operated in single-chamber conditions *J. Power Sources* **153** 108–13
[25] Yano M, Tomita A, Sano M and Hibino T 2007 Recent advances in single-chamber solid oxide fuel cells: a review *Solid State Ion.* **177** 3351–9